SMC-TR-96-17

AEROSPACE REPORT NO.
TR-96(3130)-1

Penetration of ESD Fields Through Small Apertures in the Titan IV Payload Fairing

1 March 1996

Prepared by

H.C. KOONS
Space and Environment Technology Center
Technology Operations

Prepared for

SPACE AND MISSILE SYSTEMS CENTER
AIR FORCE MATERIEL COMMAND
2430 E. El Segundo Boulevard
Los Angeles Air Force Base, CA 90245

National Systems Group

THE AEROSPACE CORPORATION
El Segundo, California

This report was submitted by The Aerospace Corporation, El Segundo, CA 90245-4691, under Contract No. F04701-93-C-0094 with the Space and Missile Systems Center, 2430 E. El Segundo Blvd., Los Angeles Air Force Base, CA 90245. It was reviewed and approved for The Aerospace Corporation by A. B. Christensen, Principal Director, Space and Environment Technology Center.

This report has been reviewed by the Public Affairs Office (PAS) and is releasable to the National Technical Information Service (NTIS). At NTIS, it will be available to the general public, including foreign nationals.

This technical report has been reviewed and is approved for publication. Publication of this report does not constitute Air Force approval of the report's findings or conclusions. It is published only for the exchange and stimulation of ideas.

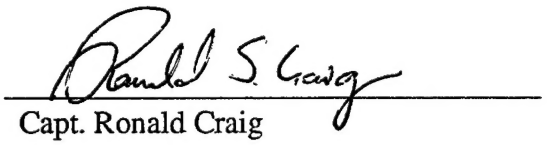

Capt. Ronald Craig
Project Officer
SMC/CLX

REPORT DOCUMENTATION PAGE

Form Approved
OMB No. 0704-0188

1. AGENCY USE ONLY (*Leave blank*)	2. REPORT DATE	3. REPORT TYPE AND DATES COVERED
	1 March 1996	

4. TITLE AND SUBTITLE
Penetration of ESD Fields Through Small Apertures in the Titan IV Payload Fairing

5. FUNDING NUMBERS
F04701-93-C-0094

6. AUTHOR(S)
Koons, Harry C.

7. PERFORMING ORGANIZATION NAME(S) AND ADDRESS(ES)
The Aerospace Corporation
Technology Operations
El Segundo, CA 90245-4691

8. PERFORMING ORGANIZATION REPORT NUMBER
TR-96(3130)-1

9. SPONSORING/MONITORING AGENCY NAME(S) AND ADDRESS(ES)
Space and Missile Systems Center
Air Force Materiel Command
2430 E. El Segundo Blvd.
Los Angeles Air Force Base, CA 90245

10. SPONSORING/MONITORING AGENCY REPORT NUMBER
SMC-TR-96-17

11. SUPPLEMENTARY NOTES

12a. DISTRIBUTION/AVAILABILITY STATEMENT
Approved for public release; distribution unlimited.

12b. DISTRIBUTION CODE

13. ABSTRACT (*Maximum 200 words*)

The new thermal protection system (TPS) for the biconic section of the Titan IV payload fairing (PLF) is a dielectric material that will electrically charge when the launch vehicle passes through clouds containing ice or snow particles. The fairing can charge to sufficiently high voltages to cause electrostatic discharges (ESD) to occur along the surface of the PLF. The Titan IV PLF has a few small openings that will serve as apertures for the entry of electromagnetic fields radiated by the discharges on the surface of the PLF. This report documents the analysis approach used to calculate the field levels on and within the PLF.

14. SUBJECT TERMS
Electrostatic Discharge
Titan IV
Triboelectric Charging

15. NUMBER OF PAGES
30

16. PRICE CODE

17. SECURITY CLASSIFICATION OF REPORT	18. SECURITY CLASSIFICATION OF THIS PAGE	19. SECURITY CLASSIFICATION OF ABSTRACT	20. LIMITATION OF ABSTRACT
UNCLASSIFIED	UNCLASSIFIED	UNCLASSIFIED	

PENETRATION OF ESD FIELDS THROUGH SMALL APERTURES IN THE TITAN IV PAYLOAD FAIRING

Introduction

The new thermal protection system (TPS) for the biconic section of the Titan IV payload fairing (PLF) is a dielectric material that will electrically charge when the launch vehicle passes through clouds containing ice or snow particles. When an ice or snow particle impacts on the fairing electrons transfer from the particle to the fairing. In this way the fairing can charge to sufficiently high voltages to cause electrostatic discharges (ESD) to occur along the surface of the PLF. This process is known as triboelectric charging or p-static charging. The "p" stands for precipitation because early aviators associated the EMI on their communications and navigation receivers with flying through precipitation.[1]

The Titan IV PLF is made of aluminum which shields the interior from external electromagnetic radiation. However, it has a few small openings that will serve as apertures for the entry of electromagnetic fields radiated by the discharges on the surface of the PLF. It is essential that the launch vehicle and the space vehicle be able to withstand the electric and magnetic field levels arising from these triboelectric discharges without any adverse affect on their performance.

The purpose of this report is to document the analysis approach used to calculate the field levels on and within the PLF. The triboelectric discharge is assumed to occur as a streamer discharge along the surface of the TPS on the conic sections of the PLF, i.e. above Station 792 in Fig. 1. The discharge is modeled as a horizontal electric dipole along the surface of the TPS. The following steps are required to calculate the fields inside the PLF: (1) the charging current density to a unit area of the PLF is determined from experimental data obtained by SRI on large aircraft operating in cirrus, stratocumulus and snow clouds,[2] (2) the discharge rate on a specified area is determined from the charging current and the average current dissipated by a single discharge,[2] (3) the SRI Static-Electricity Analysis Model is used to compute the current spectral density which is directly related to the spectral density of the electric dipole moment for the discharges occurring on the area,[3] (4) expressions for the electromagnetic fields of dipole antennas elevated over a ground plane[4] are used to compute the electric and magnetic fields at the location of an aperture which is taken to be relatively close to the area that is discharging, (5) the fields inside the PLF are obtained using a quasi-static analysis of aperture penetration developed by Bethe[5] as formulated by Taylor.[6]

Titan IV PLF Apertures

Because the charging current is minimal along the cylindrical section of the PLF, the only apertures that must be considered are those on or near to the conical sections. The apertures in the Titan IV PLF have been described by Vasile.[7] Although many small

apertures are described by Vasile, the only ones on the conical sections of the PLF that are important at the low frequencies produced by ESD are at the cone-cone junction and the cone-cylinder junction, identified as locations 2 and 3 in Fig. 1. There are three apertures at location 1 evenly spaced around the circumference of the vehicle. Each aperture, shown in Fig. 2, is 1.5 inches long by 0.010 inches wide. There are six apertures at location 2. They occur in pairs evenly spaced around the circumference of the vehicle. Each of these apertures, shown in Fig. 3, is 2.0 inches long by 0.25 inches wide. These are the largest uncovered apertures on the PLF.

Triboelectric Charging Current

Since triboelectric charging occurs when charge is transferred from an ice crystal to the PLF, the charging current depends on the density of ice crystals in the cloud, the frontal area of the vehicle, and the speed of the vehicle. At speeds in excess of 3,000 ft/sec the ice apparently turns to liquid on impact and charging does not occur.[8]

We assume that the charging current per unit frontal area is the same for the Titan IV as for a large aircraft. This assumption allows us to use SRI's studies of aircraft charging as the basis for this analysis.

First we compute the charging current per unit of frontal area. The total charging current to an airplane is given by[3]

$$I_c = 6.0757 \times 10^{-4} \cdot spdfa \cdot cloud \cdot xn \qquad (1)$$

where *spdfa* is a speed factor, *cloud* is an integer that depends on the cloud type, and *xn* is the ratio of the charging area of the vehicle to the effective charging area of a KC-135 airplane. The speed factor is:

$$spdfa = -2.345 \times 10^{-9} \cdot s^3 + 4.876 \times 10^{-6} \cdot s^2 + 6.65 \times 10^{-4} \cdot s \qquad (2)$$

where s is the speed of the vehicle in miles-per-hour. The maximum value of the speed factor in Equ. 2 is 4.067 when s = 1,451 mph or 2,134 ft/sec.

For clouds containing a small amount of charging material such as cirrus clouds, *cloud* = 1, for clouds with a moderate amount of charging material, *cloud* = 2, and for clouds with a large amount of charging material such as snow clouds, *cloud* = 4.

To obtain the charging current density we divide the total charging current by the effective charging area of the KC-135 which has been measured to be 50 ft^2 or 4.65 m^2.

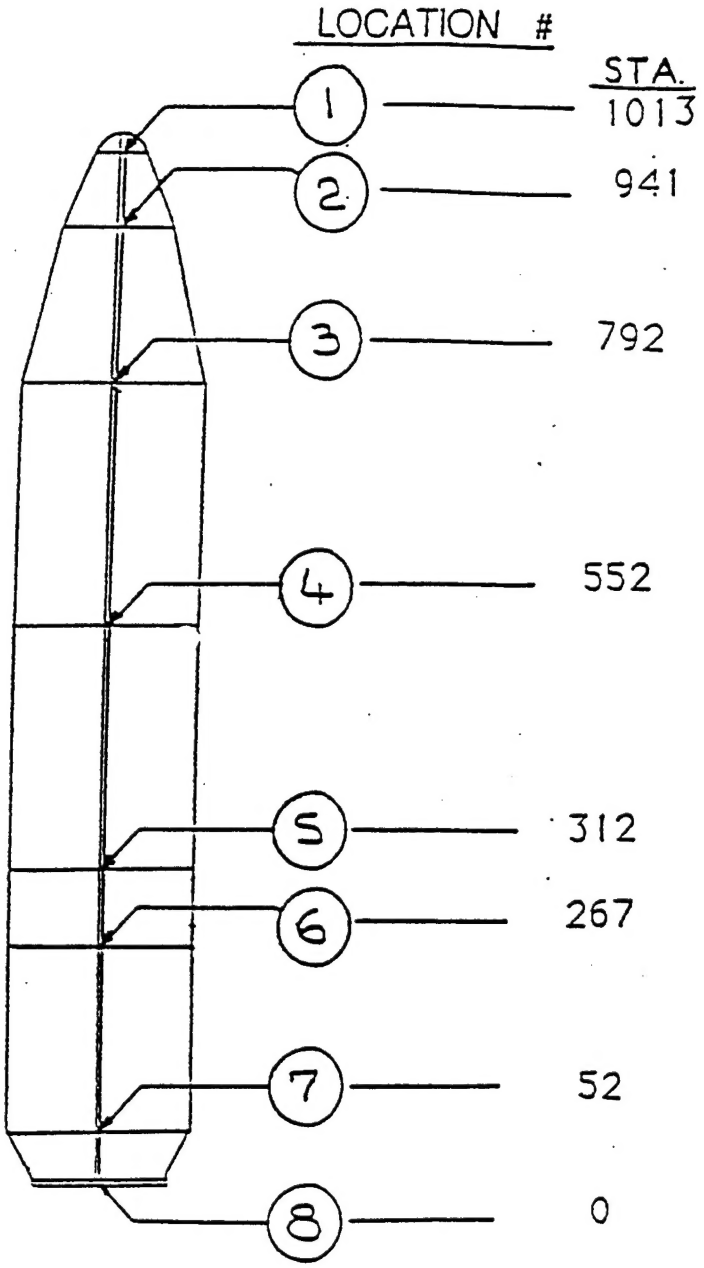

Fig. 1 The external geometry of the Titan IV payload fairing. The stations are given in inches from the base.

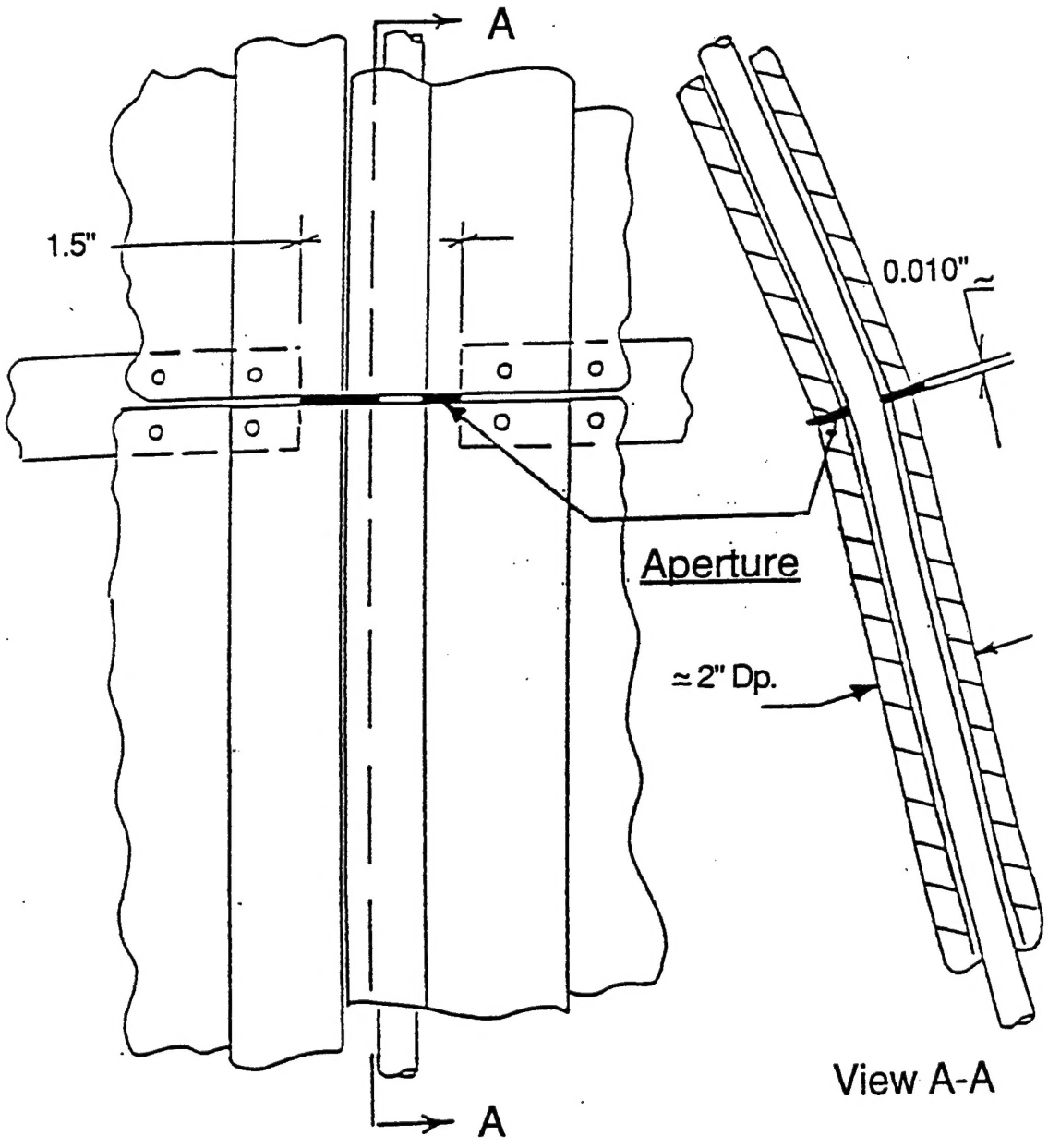

Note: No cover used at this station

Fig. 2 Apertures at the cone-cone junction (Station 941) on the PLF.

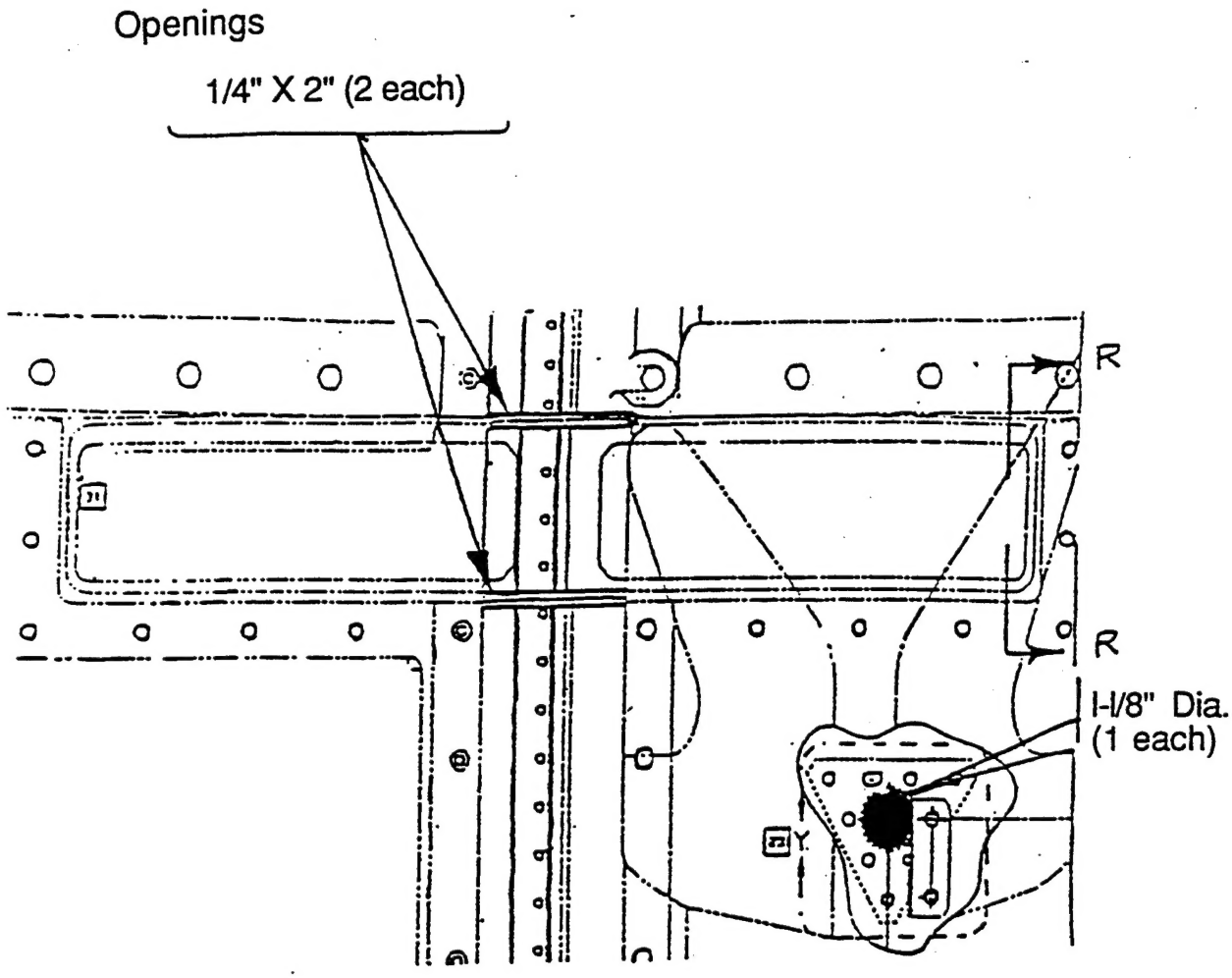

Fig. 3 Apertures at the cone-cylinder junction (Station 792) on the PLF.

Since it would be unlikely that a Titan IV would be launched during a snow storm, we use cloud = 2 for moderate charging material in this report. For clouds with a moderate amount of charging material the charging current density at the maximum value of the speed factor is then given by:

$$I_c = 6.0757 \times 10^{-4} \times 4.067 \times 2 / 4.645 = 0.001 \text{ A/m}^2 \quad (3)$$

This value will be used to compute the fields from ESD on the Titan IV PLF. If launched through snow clouds the charging current would be twice as large.

In order to make use of the noise-spectra equations derived by SRI, we will use a rectangular area of length, L, and width, W. We will orient this area with its length horizontal, i.e. at a constant PLF station. We will also use the maximum width analyzed by SRI, W = 0.3 m. In their analysis they show that the result is essentially independent of the length of the discharging area. We imagine the PLF as made up of a very large number of such areas and will show that areas away from the aperture produce negligible noise inside the PLF.

The charging current to a physical area is obtained by multiplying the effective area, i.e. the actual frontal area times the charging efficiency, by the charging current density given by Equ. 3. The charging efficiency of an area is only 20% to 25% of its physical frontal area.[2] The frontal area is the area projected normal to the velocity vector. At the cone-cone junction on the Titan IV the angle between the area normal and the vehicle axis is 65 deg (the complement of 25 deg) as shown in Fig 4. At the cone-cylinder junction that angle is 75 deg. If we take the length, L, of our sample area to be 0.6 m and use the maximum area efficiency of 25% then the charging current to our sample area at the cone-cone junction is 19 μA and at the cone-cylinder junction it is 11.6 μA.

Discharge Rate

An average discharge current is 1.5×10^{-9} A.[2] If we divide the charging current to our sample area by this average current we obtain the discharge rate, ν, on our sample area. At the cone-cone junction the discharge rate is

$$\nu = \frac{19 \times 10^{-6}}{1.5 \times 10^{-9}} = 1.27 \times 10^{4} \text{ per second} \quad (4)$$

and similarly at the cone-cylinder junction the rate is 773 discharges per second.

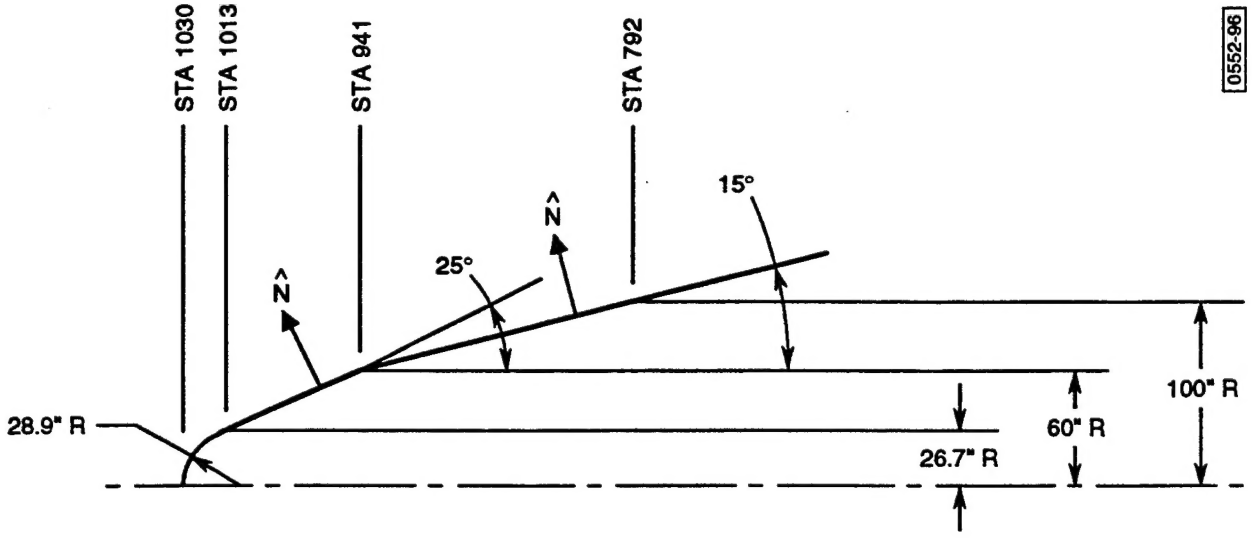

Fig. 4 Geometry of the Titan IV cone-cone and cone-cylinder junctions. The symbol $\hat{N}$ identifies the unit vectors normal to the surfaces on the conical sections.

Noise Power Spectrum

The short-circuit current noise-power spectrum induced in an antenna by a series of streamer pulses is[2]

$$G(\omega) = \frac{\nu I_m^2 v^2}{\pi} |g(\omega)|^2 \overline{|f(x,l)|^2} \tag{5}$$

where I_m is the peak value of the current flowing in the discharge, v is the velocity of propagation of the discharge, and ν is the average rate of occurrence of the streamers. The term $|g(\omega)|^2$ is the square of the Fourier transform of the basic streamer function:

$$g(t) = \frac{a}{\alpha}\left(1 - e^{-\alpha t}\right) + \frac{b}{\beta}\left(1 - e^{-\beta t}\right) \tag{6}$$

Thus

$$|g(\omega)|^2 = \frac{\omega^2 (a+b)^2 + (a\beta + b\alpha)^2}{\left(\alpha^2 + \omega^2\right)\left(\beta^2 + \omega^2\right)} \tag{7}$$

For a typical streamer,

$a = 0.597$
$b = 0.403$
$\alpha = 1.67 \times 10^7\ s^{-1}$
$\beta = 3.47 \times 10^6\ s^{-1}$
$I_m = 0.01$ A

The term $\overline{|f(x,l)|^2}$ is an ensemble average of the coupling term over the discharges occurring on a particular surface. For a rectangular area[2]

$$\overline{|f(x,l)|^2} = 2\Psi^2 \left[1 - \frac{\sin \frac{W}{2v}\omega}{\frac{W}{2v}\omega} \right] \tag{8}$$

Here Ψ is the coupling term between the discharge and the receiver. It is at this point that we diverge from the formulation of Nanevicz and Douglas. Instead of treating the problem as a direct coupling problem, we use Equ. 5 as the source current noise power

spectrum and we will explicitly calculate the coupling using electromagnetic propagation equations from the source to the aperture and from the aperture to the interior of the PLF. Since Ψ is a function only of the geometry and not of the discharge parameters we can replace Ψ by multiplicative factors representing the more complicated geometry in our problem. A limitation in our approach that is also present in the formulation by Nanevicz and Douglas is that the distance to the aperture should be much larger than the width, W, of a sample area. This allows Ψ to be taken out from under an integral over the dielectric surface on which charging occurs. In order to obtain a tractable solution we assume that the coupling over the entire surface is equal to the value of the coupling at the geometrical center of the surface. We will show the results as a function of the distance from the center of the surface to the aperture. As this distance increases the calculations will become more accurate.

Fig. 5 shows $\sqrt{G(\omega)}$ vs. frequency obtained from Equs. 5 to 8 for our sample surfaces near the cone-cone and the cone-cylinder junctions on the PLF. The difference between the curves is caused by the difference in the frontal areas due to the differing cone angles. The numeric values have been converted to conventional EMC units of amps/MHz.

Propagation Equations

The streamer discharges across the surface are modeled as horizontal electric dipoles (HED). In particular the discharges on the 0.6 m $\times$ 0.3 m surface are modeled as a single dipole located at the geometric center of the surface. The surface is taken to be centered directly above the aperture and the dipole is pointed downward directly toward the aperture as shown in Fig. 6. This simulates the streamering discharges which will tend to move downward in the direction of the air stream along the surface of the vehicle. It also represents the worst-case discharge geometry.

We will use equations developed by Bannister, who used finitely conducting earth-image theory techniques, to determine the fields at the location of the aperture from the dipole "antenna" at the center of our discharging surface.[4] Using complex image theory techniques Bannister derived simple expressions for the electric and magnetic fields produced by antennas located over the Earth's surface, for both single-layered and multilayered conducting material. In his case the material was the Earth. In our case, it is the aluminum PLF. His equations cover an arbitrarily near range as long as the material is sufficiently conducting. In our case we take the conductivity of the aluminum PLF to be ∞. The TPS is taken to be 0.25 in thick and the electric dipole is on the outer surface of the TPS. The inner surface of the TPS is in contact with the PLF. Since the HED is only 0.25 in above the conducting "ground plane" it is an extremely inefficient radiator.

The only component of the electric field at the surface of the PLF in the absence of an aperture is the normal electric field, E_z.. It is the field that would be present at the location of the aperture if the aperture were not present. It is also the external field used in Bethe's formulation for the fields inside the aperture in the presence of an aperture. We use the

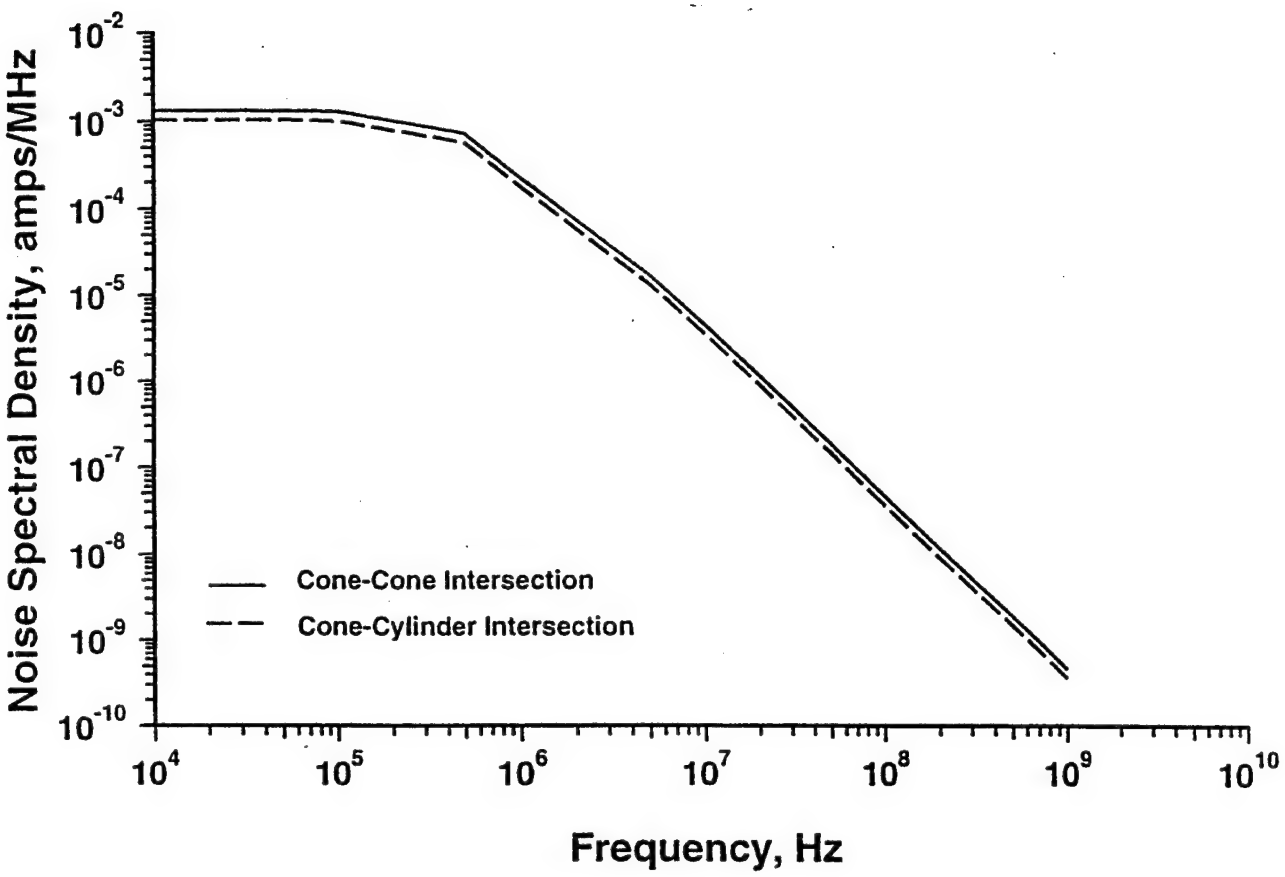

Fig. 5 Noise spectrum, $\sqrt{G(\omega)}$ vs. Frequency, for discharges on surfaces near the cone-cone and the cone-cylinder intersections on the PLF.

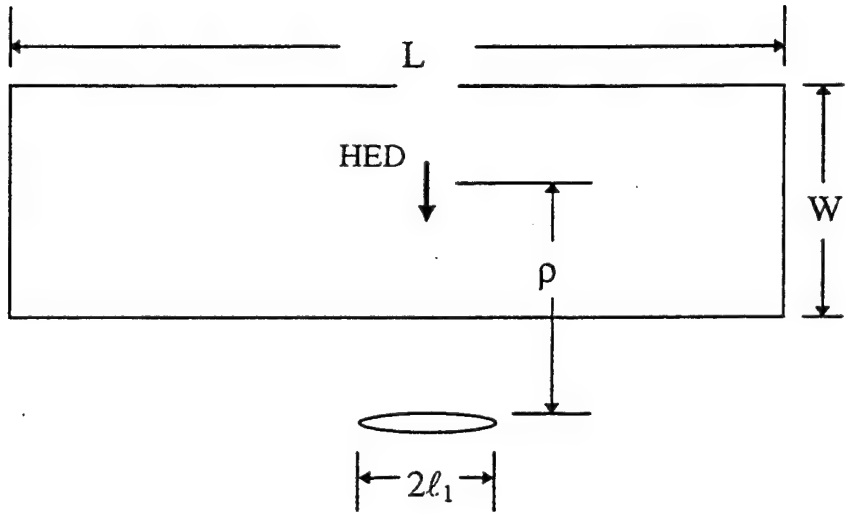

Fig. 6 Geometry used to model the horizontal electric dipole and the aperture in the PLF.

following equations simplified from Bannister's equations for our geometry for the electric and magnetic fields on the surface of the PLF:[4]

$$E_z = \frac{-I_{HED} \cdot dL_{HED} \cdot \cos\phi}{4\pi i\omega\varepsilon_0} \left[(3+3\gamma_0 D)\sin\Psi + \gamma_0^2 D^2 \sin\Psi_1\right]\frac{\exp(-\gamma_0 D)}{D^3} \quad (9)$$

$$H_\phi = \frac{I_{HED} \cdot dL_{HED} \cdot \cos\phi}{2\pi} \left[D\cdot\sin\Psi + \gamma_0 D^2 \sin\Psi_1\right]\frac{\exp(-\gamma_0 D)}{D^3} \quad (10)$$

In these equations E_z is normal to the surface and H_ϕ is parallel to the surface along the major dimension of the aperture. I_{HED} is the dipole current which is taken to be $\sqrt{G(\omega)}$, dL_{HED} is the length of the dipole, ϕ is the angle between the dipole axis and the direction vector from the dipole to the aperture which in our case is 0°, γ_0 is the propagation vector in free space, D is the distance from the dipole to the aperture, and Ψ and Ψ_1 are elevation angles. For fields at the surface of the conductor $\Psi = \Psi_1 = \tan^{-1}(h/\rho)$ where h is the height of the dipole above the surface and ρ is the distance from the dipole along the surface to the aperture in cylindrical coordinates. We have evaluated Equs. 9 and 10 for the fields that would be present at the location of the aperture if it were not present. The results are given in Fig. 7 for an aperture at the cone-cone junction and in Fig. 8 for one at the cone-cylinder junction. There is only a small difference between the external fields at the apertures for the two locations. This difference is caused by the difference in the charging currents.

Field Penetration Through a Small Aperture

We use Taylor's formulation of the problem for the penetration of electromagnetic fields through a small aperture.[6] According to this formulation, which follows the quasi-static approximation first developed by Bethe,[5] the field distribution in the aperture is that which would exist if the aperture were immersed in static electric and magnetic fields apart from the overall sinusoidal time dependence. This approximation requires that the maximum linear dimensions of the aperture be very small compared with the operating wavelength. This is the case for the ESD fields generated by discharges on the PLF. The penetration fields inside the PLF at distances that are large compared with the maximum linear dimension of the aperture may then be expressed in terms of equivalent electric and magnetic dipole moments located at the center of the aperture. This analysis is not valid for fields very close to the aperture. The aperture is modeled as an elliptically shaped hole in a perfectly-conducting infinitesimally-thin sheet. The z axis is directed perpendicular to the sheet and the x axis is directed parallel to the major dimension of the aperture. The x direction thus corresponds to the φ direction in the field calculation in the preceding section. For a small aperture the penetration fields are expressed in terms of the dipole moments of equivalent magnetic charge and current distributions in the aperture. A

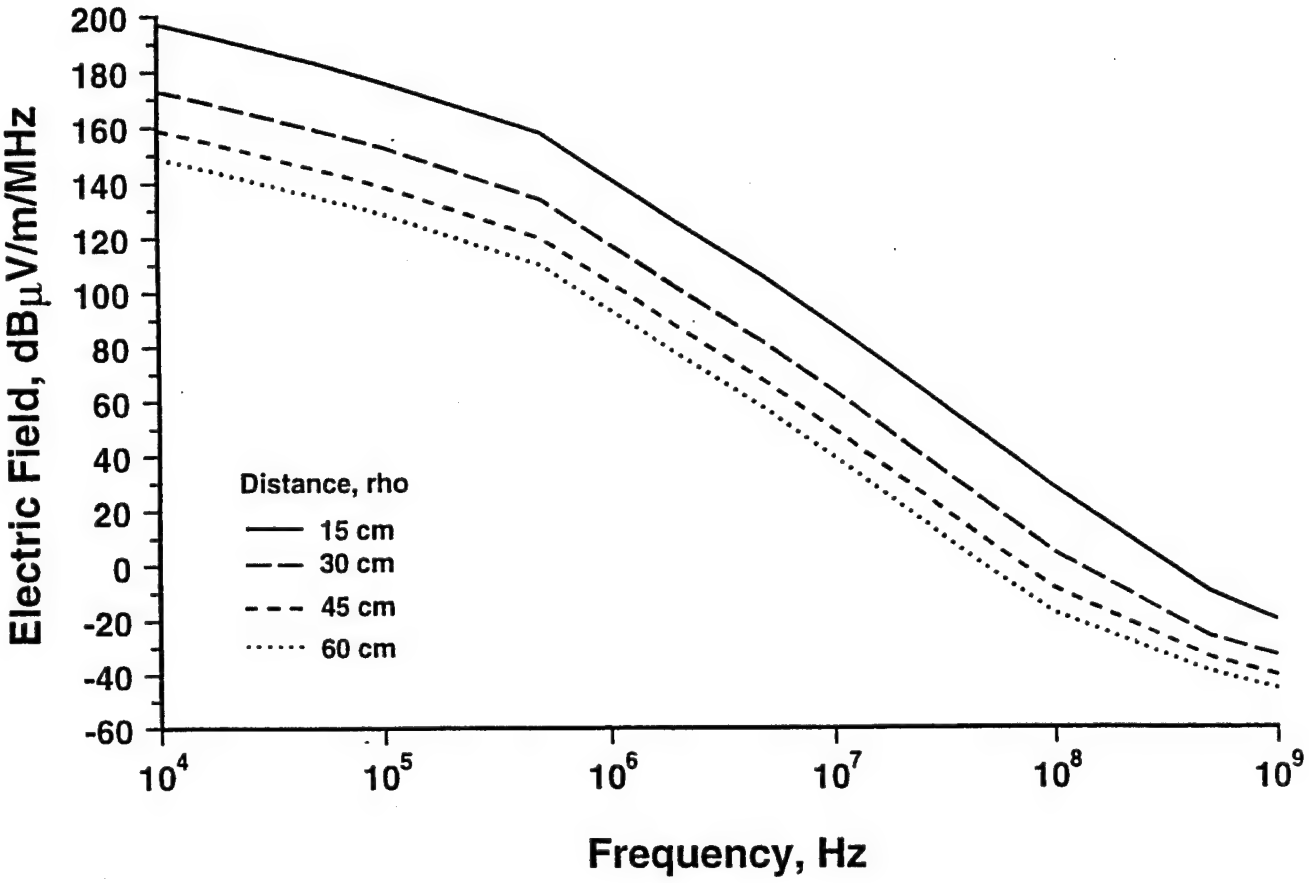

Fig. 7 Vertical electric field at the aperture at the cone-cone junction as a function of the distance of the discharging surface from the aperture.

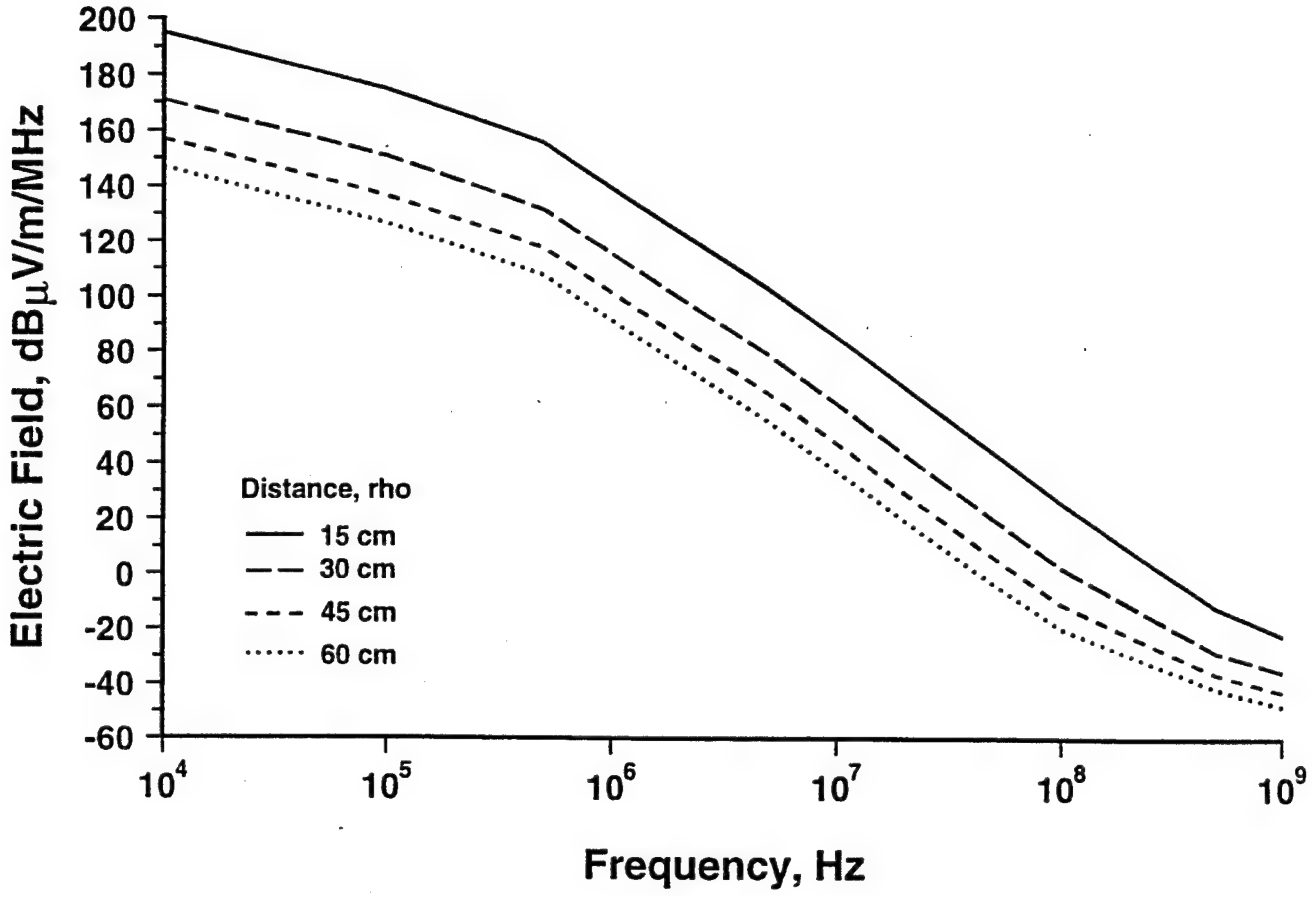

Fig. 8 Vertical electric field at the aperture at the cone-cylinder junction as a function of the distance of the discharging surface from the aperture.

dyadic, $\vec{\alpha}$, relates these dipole moments, $\vec{M}_0$ and $\vec{P}_0$, of the aperture field distribution to the magnetic field strength, $\vec{H}_0$, and the electric flux density, $\vec{D}_0$, that would exist at the position of the aperture if it were not present.

$$\vec{M}_0 = \vec{\alpha} \cdot \vec{H}_0 \tag{11}$$

$$\vec{P}_0 = \vec{\alpha} \cdot \vec{D}_0 \tag{12}$$

The elements of the dyadic for an elliptical aperture are

$$\alpha_{11} = -\frac{2\pi}{3} \frac{\ell_1^3 e^2}{K(e^2) - E(e^2)} \tag{13a}$$

$$\alpha_{22} = -\frac{2\pi}{3} \frac{\ell_1^3 e^2 (1-e^2)}{E(e^2) - (1-e^2) K(e^2)} \tag{13b}$$

$$\alpha_{33} = +\frac{2\pi}{3} \frac{\ell_1^3 (1-e^2)}{E(e^2)} \tag{13c}$$

$$\alpha_{ij} = 0, \qquad i \neq j \tag{13d}$$

where $E(e^2)$ and $K(e^2)$ are elliptical integrals of the first and second kinds, respectively, e is the eccentricity of the aperture, and ℓ_1 is the half-length of its semimajor axis.[6]

At the frequencies of concern (< 10 MHz) the wavelength, λ, is much greater than the distance, R, from the aperture to the observation point. On the line through the center of the aperture and normal to the surface, the fields in the interior are then given by

$$\vec{E}' = E_z' = \frac{\alpha_{33} E_z}{2\pi R^3} \tag{14}$$

and

$$\vec{H}' = H_\phi' = \frac{\alpha_{11} H_\phi}{4\pi R^3} \tag{15}$$

These can be recognized as the near fields of the electric and magnetic dipoles respectively. General expressions for the interior field can be found in Taylor's paper.[6]

Validation of Taylor's Analysis

In order to verify the theory of the penetration of fields through a gap we have compared the field intensities calculated using Taylor's equations to controlled laboratory measurements by Honig.[9] Honig measured the shielding effectiveness of steel sheets with variable length slots. The shielding effectiveness is defined as the ratio in decibels of the field that would be present at an interior observation point in the absence of a barrier to the field that is present there in the presence of a barrier with an aperture. The slots were cut in a plate which formed part of the wall of an electromagnetically shielded enclosure (a screen room). The slots were 1/16 in wide and varied from 0.2 to 12 in long. A magnetic loop antenna on the outside of the enclosure generated an ac magnetic field and a magnetic loop antenna on the inside of the enclosure measured the field that penetrated the aperture. The geometry is shown in Fig. 9. The dipoles were oriented such that the magnetic field at the slot was directed parallel to the long axis of the slot. The magnetic loops were each located a distance of 12 in from the aperture. The measurement results from Fig. 8 in Honig's paper are shown in Fig. 10 for 10 kHz and 1 MHz. Very little dependence on frequency was observed over this range.

The equations for this geometry differ from those for the PLF because the source is a magnetic dipole above the surface. If $\vec{M}_1$ is the dipole moment of the source antenna a distance R_1 from the aperture and $\vec{M}_1$ is oriented such that the dipole moment points in the +x direction, then at the aperture

$$\vec{H}_0 = H_0\hat{x} = \frac{-M_1\hat{x}}{4\pi R_1^3} \tag{16}$$

Assuming that ℓ_1 is parallel to $\hat{x}$, the equivalent dipole moment of the aperture field distribution is

$$\vec{M}_0 = \alpha_{11}\vec{H}_0 \tag{17}.$$

and the field at the receiving antenna a distance R_2 from the aperture in the presence of the barrier is

$$\vec{H}_2 = -\frac{M_0\hat{x}}{4\pi R_2^3} = -\frac{\alpha_{11}H_0\hat{x}}{4\pi R_2^3} = +\frac{\alpha_{11}M_1\hat{x}}{16\pi^2 R_1^3 R_2^3} \tag{18}$$

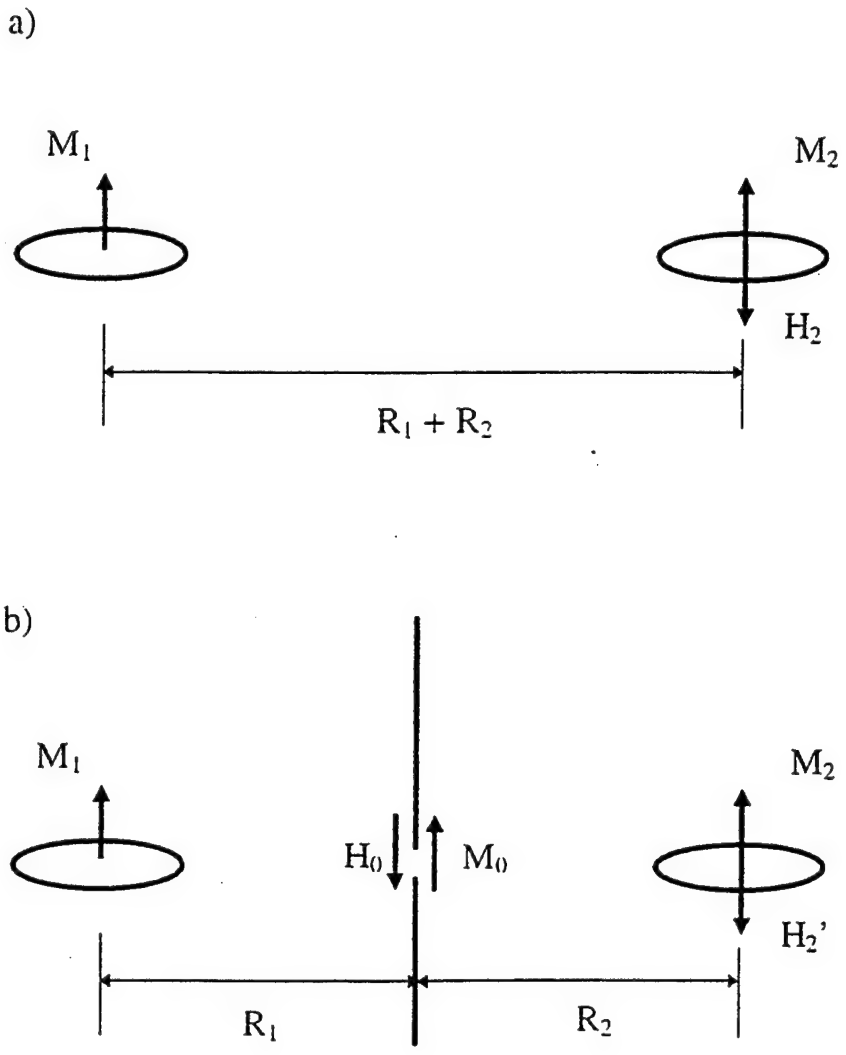

Fig. 9 Magnetic loop antenna and slot geometry for Honig's shielding effectiveness measurements. (a) geometry without a barrier. (b) geometry with a barrier containing an aperture.

In the absence of the barrier

$$\vec{H}_2 = +\frac{M_1 \hat{x}}{4\pi(R_1 + R_2)^3} \tag{19}$$

The shielding effectiveness of the slot then is given by the ratio

$$\frac{|H_2|}{|H_2'|} = \frac{\alpha_{11}(R_1 + R_2)^3}{4\pi R_1^3 R_2^3} \tag{20}$$

Equation 20 was used to calculate the shielding effectiveness for Honig's measurements. The results are shown as the solid line in Fig. 10. The agreement is excellent for slot lengths less than 4 in and for a slot length of 12 in. In fact Honig's measured values at 4, 5 and 10.5 in may be inaccurate because there is no reason to expect the shielding effectiveness to increase only over this range as it does in his measurements. The agreement of the data with Honig's data also shows that the approximations used in our analysis are quite accurate for fields below 1 MHz at a distance of 12 in (30 cm) inside the aperture. The requirement that $R << \lambda$ places an upper limit on the frequency of 30 MHz at 10 cm and 100 MHz at 30 cm. Since the agreement of the theory with Honig's observations is quite good at R = 12 in for a slot that is 12-in long, the theory should also be good at R= 4 in (10 cm) for a slot that is 4-in long or less. Thus the error for the largest PLF aperture which is 2.0-in long is most likely less than 10 dB at 10 cm inside the fairing.

Fields in the Interior of the PLF

The electric fields at 10 cm and 30 cm inside the PLF are shown in Fig. 11 for one of the large apertures at the cone-cylinder junction. The fields from one 0.6 m × 0.3 m discharging area are plotted for the closest outside distance from the center of the discharging area to the center of the aperture. The closest distance is 15 cm since the width of the area has been taken to be 30 cm. Fig. 12 shows a similar plot for one of the small apertures at the cone-cone junction. The much larger fields interior to the cone-cylinder junction (Fig. 11) result from the much larger hole there.

The next closest area will be centered 45 cm from the aperture. From Figs. 12 and 13 we see that the fields from this area are down almost 40 dB from the fields from the area immediately adjacent to the aperture. This means that only discharges on the closest area need be considered in the analysis.

The power flux inside of the vehicle is given by the Poynting vector which is

$$\vec{S} = \vec{E}_2 \times \vec{H}_2 = E_z' \cdot H_\phi' \tag{21}$$

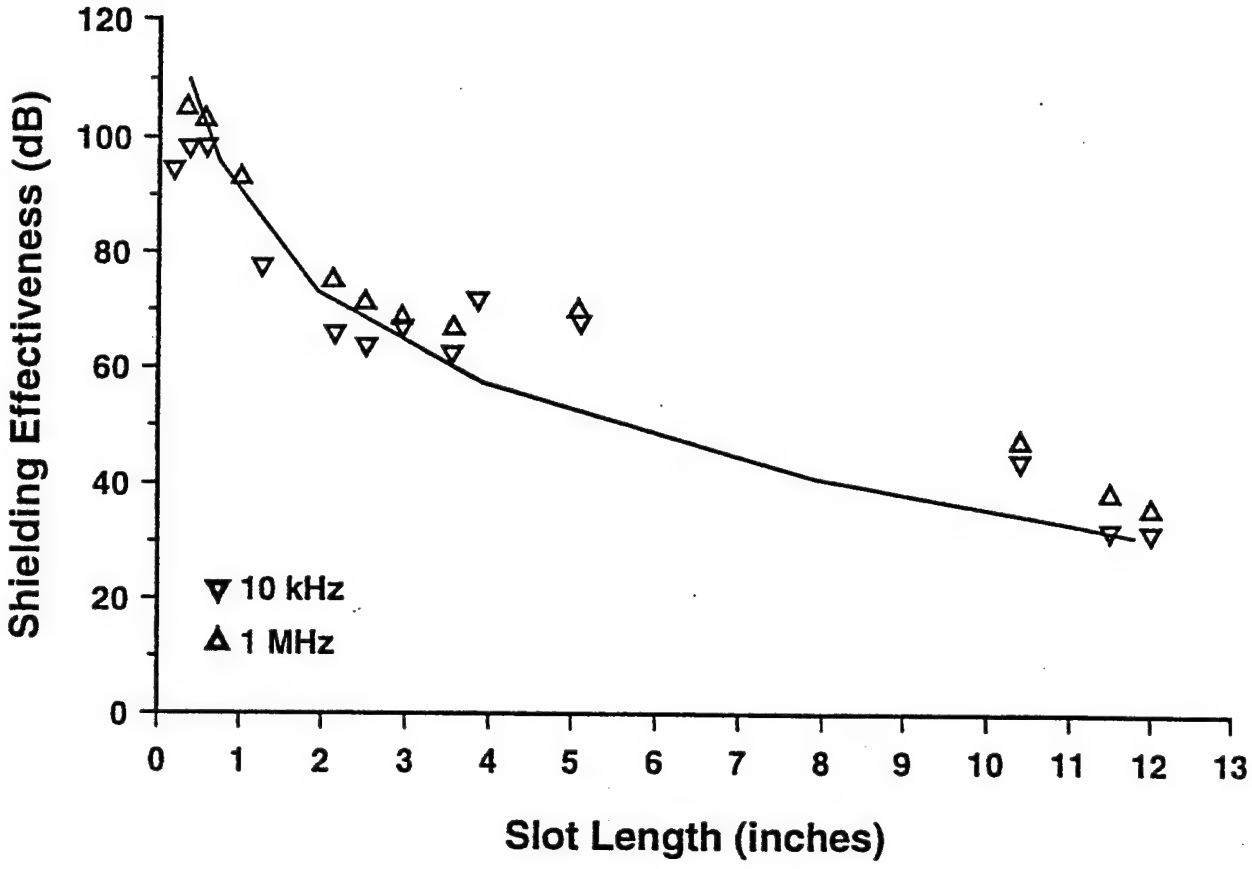

Fig. 10 Comparison of theoretical results (solid curve) with Honig's shielding effectiveness measurements for Honig's magnetic loop antenna geometry.

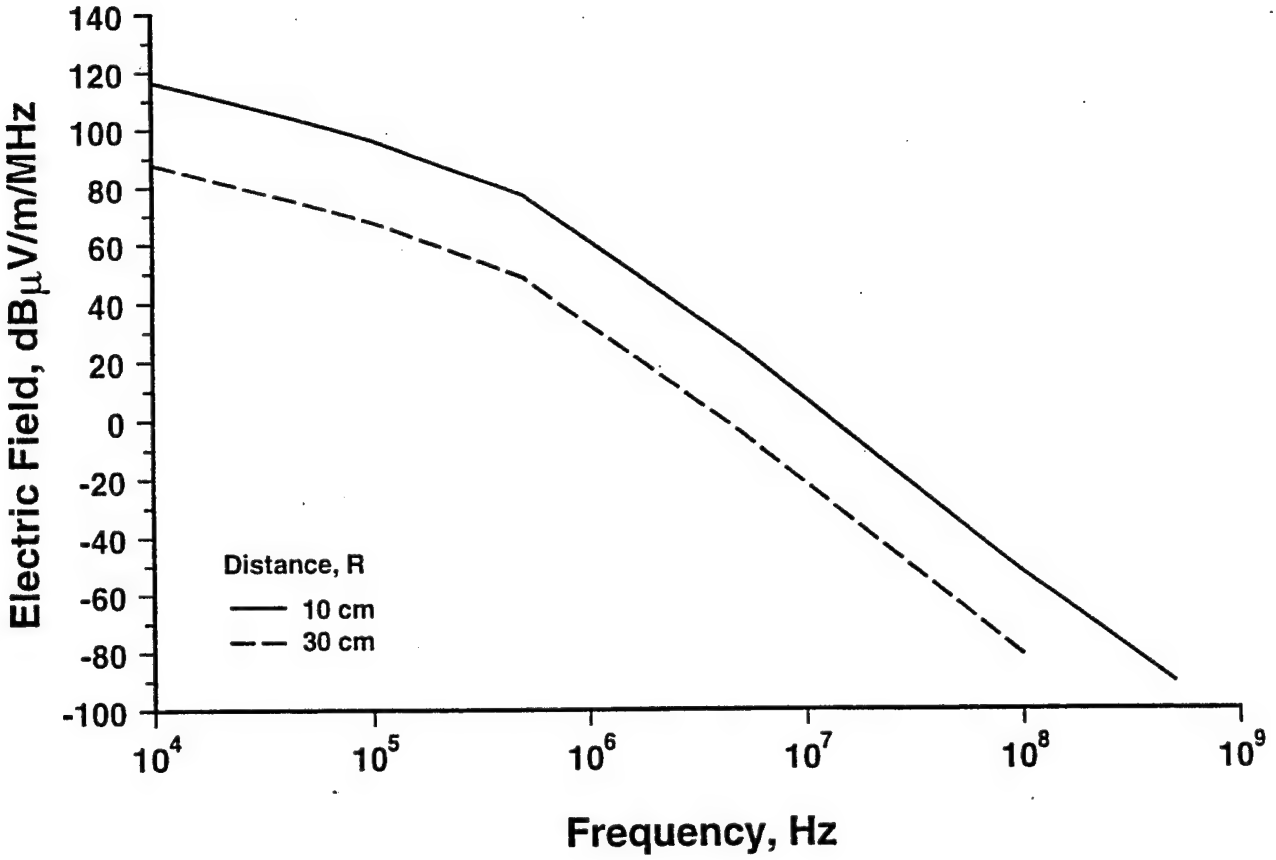

Fig. 11 The electric fields at 10 cm and 30 cm inside the PLF for a large aperture at the cone-cylinder junction.

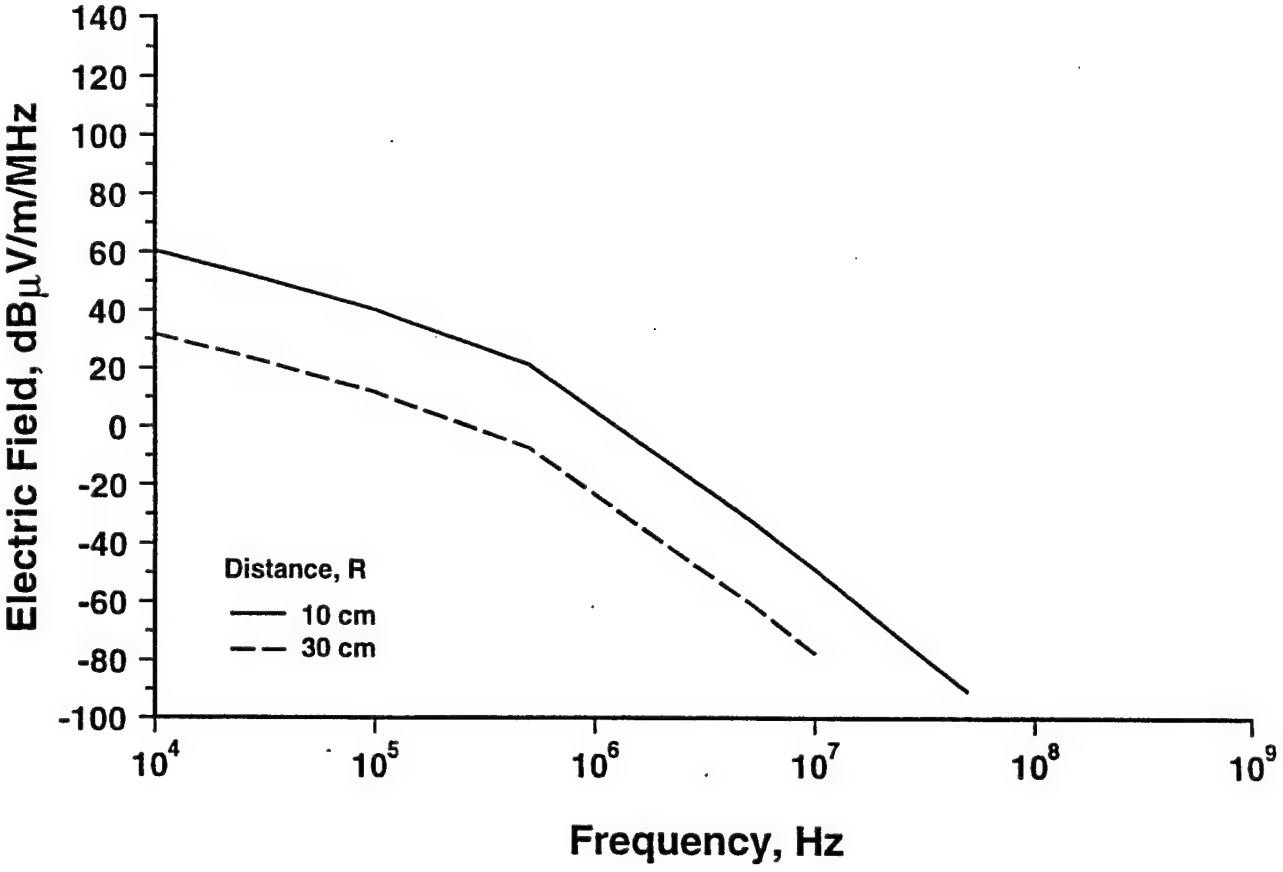

Fig. 12 The electric fields at 10 cm and 30 cm inside the PLF for a small aperture at the cone-cone junction.

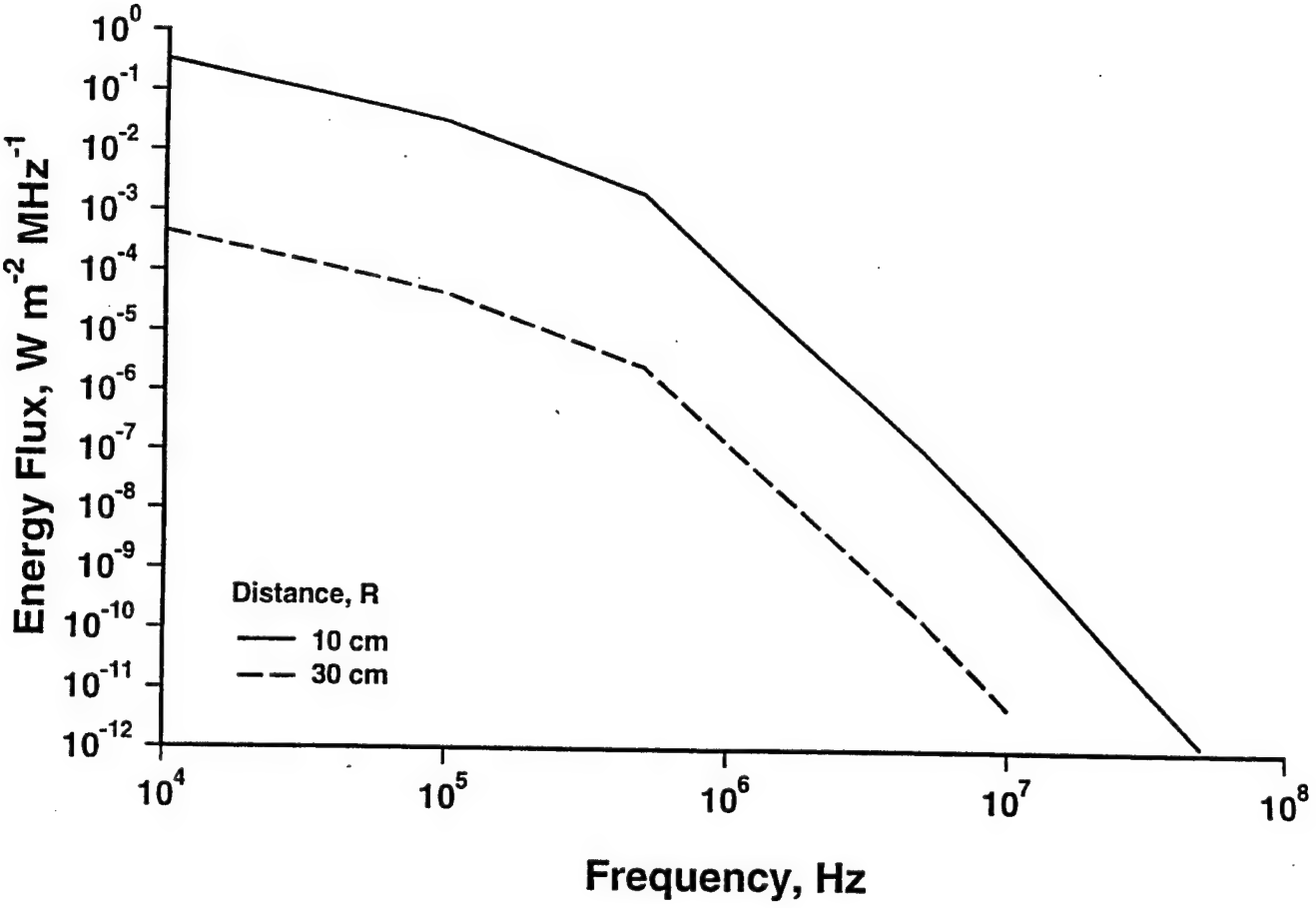

Fig. 13 The Poynting flux at 10 cm and 30 cm inside the PLF for a large aperture at the cone-cylinder junction.

The magnitude of S at 10 cm and 30 cm inside the PLF on the axis of the aperture is shown in Fig. 13 for a large aperture at the cone-cylinder junction. Fig. 14 shows a similar plot for a small aperture at the cone-cone junction.

Accuracy

Taylor[6] states that the quasi-static analysis breaks down at penetration field distances that are not long compared with the maximum linear dimension of the aperture. However, Fig. 10 shows that there is good agreement between theory and measurement for a 12-in slot when the measurements were made at a penetration field distance of 12 in. In fact at 1 MHz it shows that theory predicts a larger field than was actually measured. This suggests that the theory can be used to predict maximum fields at distances comparable to the maximum linear dimension of the aperture. In the PLF application that would be at 2 in from the larger aperture.

The fields calculated here are for an ideal aperture in an ideal conducting sheet. The real apertures shown in Fig. 2 and 3 are more complicated because of the finite thickness and more complex geometry of the PLF. Since the approximations used in this analysis apply only to wavelengths much greater than the distances and dimensions involved on the PLF, the results should be accurate to better than an order of magnitude for these more complex geometries.

An obvious way to further decrease the electric fields within the PLF is to decrease the dimensions of the apertures.

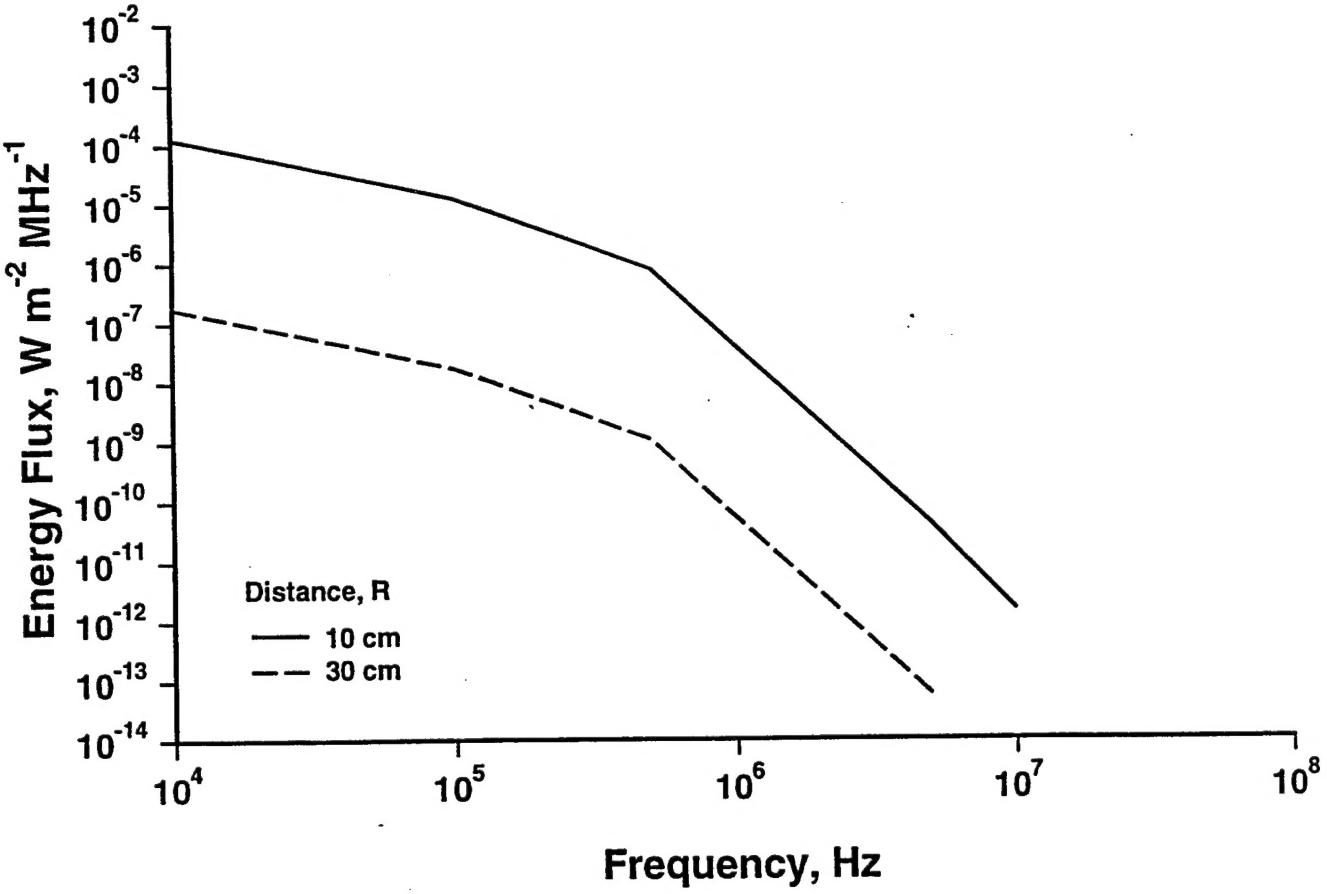

Fig. 14 The Poynting flux at 10 cm and 30 cm inside the PLF for a large aperture at the cone-cone junction.

References

1. H. M. Hucke, "Precipitation-Static Interference on Aircraft and at Ground Stations", *Proc. IRE, 27,* 301-316, 1939.

2. J. E. Nanevicz and D. G. Douglas, "Static-Electricity Analysis Program: Final Report - Volume I," *SAMSO TR 75-44,* Space and Missile Systems Organization, Los Angeles, CA, Oct. 1974.

3. D. G. Douglas and J. E. Nanevicz, "Static-Electricity Analysis Program: Users Manual - Volume II," *SAMSO TR 75-44,* Space and Missile Systems Organization, Los Angeles, CA, Oct. 1974.

4. P. R. Bannister, "Extension of Finitely Conducting Earth-Image-Theory Results to Any Range," *Technical Report 6885,* Naval Underwater Systems Center, New London Laboratory, New London, CT, 11 Jan. 1984.

5. H. A. Bethe, "Theory of Diffraction by Small Holes," *Phys. Rev., 66,* 163-182, 1944.

6. C. D. Taylor, "Electromagnetic Pulse Penetration Through Small Apertures," *IEEE Trans. EMC, EMC-15,* 17-26, 1973.

7. G. M. Vasile, "Shielding Effectiveness of S/N 29 Payload Fairing after Installation of the Shielding Kit," *McDonnell Douglas Report MDC 92H0823,* McDonnell Douglas Astronautics Company, Huntington Beach, CA, May 1992.

8. Launch Vehicle Lightning/Atmospheric Electrical Constraints Post-Atlas/Centaur 67 Incident, *Aerospace Report No. TOR-0088(3441-45)-2,* The Aerospace Corporation, El Segundo, CA, 31 August 1988, p. 3-45.

9. E. M. Honig, Jr., "Electromagnetic Shielding Effectiveness of Steel Sheets with Partly Welded Seams," *IEEE Trans. EMC, EMC-19,* 377-382, 1977.

TECHNOLOGY OPERATIONS

The Aerospace Corporation functions as an "architect-engineer" for national security programs, specializing in advanced military space systems. The Corporation's Technology Operations supports the effective and timely development and operation of national security systems through scientific research and the application of advanced technology. Vital to the success of the Corporation is the technical staff's wide-ranging expertise and its ability to stay abreast of new technological developments and program support issues associated with rapidly evolving space systems. Contributing capabilities are provided by these individual Technology Centers:

Electronics Technology Center: Microelectronics, VLSI reliability, failure analysis, solid-state device physics, compound semiconductors, radiation effects, infrared and CCD detector devices, Micro-Electro-Mechanical Systems (MEMS), and data storage and display technologies; lasers and electro-optics, solid state laser design, micro-optics, optical communications, and fiber optic sensors; atomic frequency standards, applied laser spectroscopy, laser chemistry, atmospheric propagation and beam control, LIDAR/LADAR remote sensing; solar cell and array testing and evaluation, battery electrochemistry, battery testing and evaluation.

Mechanics and Materials Technology Center: Evaluation and characterization of new materials: metals, alloys, ceramics, polymers and composites; development and analysis of advanced materials processing and deposition techniques; nondestructive evaluation, component failure analysis and reliability; fracture mechanics and stress corrosion; analysis and evaluation of materials at cryogenic and elevated temperatures; launch vehicle fluid mechanics, heat transfer and flight dynamics; aerothermodynamics; chemical and electric propulsion; environmental chemistry; combustion processes; spacecraft structural mechanics, space environment effects on materials, hardening and vulnerability assessment; contamination, thermal and structural control; lubrication and surface phenomena; microengineering technology and microinstrument development.

Space and Environment Technology Center: Magnetospheric, auroral and cosmic ray physics, wave-particle interactions, magnetospheric plasma waves; atmospheric and ionospheric physics, density and composition of the upper atmosphere, remote sensing using atmospheric radiation; solar physics, infrared astronomy, infrared signature analysis; effects of solar activity, magnetic storms and nuclear explosions on the earth's atmosphere, ionosphere and magnetosphere; effects of electromagnetic and particulate radiations on space systems; space instrumentation; propellant chemistry, chemical dynamics, environmental chemistry, trace detection; atmospheric chemical reactions, atmospheric optics, light scattering, state-specific chemical reactions and radiative signatures of missile plumes, and sensor out-of-field-of-view rejection.